Emission of an intense electromagnetic field in a plasma-loaded-wiggler free electron device

K. H. Tsui and A. Serbeto
Instituto de Fisica, Universidade Federal Fluminense, Gragoata 24210-340, Niteroi, Rio de Janeiro, Brazil
(Received 23 March 1998)

The use of a plasma-loaded-wiggler free electron device to generate terahertz intense electromagnetic waves is analyzed. The interaction among the beam (B), the space charge mode (L), the wiggler (W), and the electromagnetic field (S) is through the simultaneous operation of the Raman (LWS) and the free electron laser (BWS) interactions warranted by having the phase velocity of the space charge beam-plasma mode equal to the free electron laser resonant beam velocity. The high-frequency space charge mode, with low beam-plasma density ratio, is generated principally by the ponderomotive force of the wiggler and the electromagnetic field through LWS coupling. On the other hand, the coupling of the space charge field and the wiggler provides the LWS channel to drive the electromagnetic field. Also, the interaction of the electron beam with the wiggler amounts to the BWS channel of driving the electromagnetic field. The electron beam in this $LBWS$ four-entity interaction is represented by either a fluid model or a single-particle model. The results of these two models are compared and discussed. [S1063-651X(98)12910-0]

PACS number(s): 41.60.Cr, 52.75.Ms

I. INTRODUCTION

Free electron lasers operating in free space are currently investigated in laboratories as an effective means of generating intense electromagnetic waves [1,2]. The interaction takes place when the Doppler shifted wave frequency in the electron beam frame matches the wiggler frequency. The driving term in the wave equation of the electromagnetic field is due to the nonlinear transverse current because of the electron bunching in the ponderomotive potential well. Here, we consider a plasma-loaded-wiggler free electron device to generate terahertz high-frequency fields [3–8]. Szu [3] considered the interaction of an electron beam with a background plasma, generated by a head on high-intensity carbon dioxide laser beam, with and without an axial magnetic field. The Raman backscattered electromagnetic mode constitutes the operation of this free electron device. Since the laser acts in the place of a mechanical wiggler, this system employs an electromagnetic wiggler loaded with a background plasma. Since the output frequency is in the same range of the wiggler, this system explores specifically the tunability of the scattering mechanism. Bobin [4] considered the working of an electron beam under a plasma-loaded mechanical wiggler with a laser field. In this system, the electron beam could be accelerated should the laser field be the primary energy source. Conversely, a high-frequency laser field could be generated should the electron beam be the primary source. Wen-Bing and Ya-Shen [5] analyzed the plasma-loaded free electron laser system and concluded that the laser gain in the Raman regime could be greatly enhanced when the background plasma density was below a critical limit. Tripathi and Liu [6] introduced a strong axial magnetic field in the loading plasma in order to obtain favorable operating parameters for the plasma-loaded-wiggler free electron device. Without the magnetic field, the phase velocity of the beam-plasma mode is larger than the speed of light. The coupling with the laser mode, therefore, requires both highly energetic beams and very small wiggler periods. With the magnetic guide field, coupling can be fulfilled with less stringent parameters for the same laser mode frequency by engaging with the transverse modes of the magnetized beam-plasma dispersion relation. Serbeto and Alves [7], and Petrillo *et al.* [8] studied the same system taking into consideration the finite temperature of the background plasma in a fluid model. The space charge dispersion relation is the temperature corrected Langmuir mode, not the beam-plasma mode. In this sense, the beam density has to be very much lower than the plasma density to avoid the excitation of the beam-plasma mode, which is the so-called weak beam case, and is the limitation of their analysis. As for the approach, Refs. [5,6] consider the periodic wiggler magnetic field as part of the background plasma equilibrium, and linear growth rate analysis is used to evaluate the dispersion relation of this system. In Refs. [4,7,8], the background plasma equilibrium is unmagnetized. The wiggler field and the laser field are treated on the same basis as perturbations. The linear growth of the nonlinear parametric process is then calculated, whereas Ref. [8] also evaluates the nonlinear saturation levels of the system.

Here, we examine the plasma-loaded-wiggler free electron laser system anew, where the electron beam is modeled by and compared with the fluid and the single-particle descriptions. Nonlinear parametric analysis is used and saturation levels are calculated. Beam density is assumed to be dense enough to drive the beam-plasma mode and to withstand a perturbation amplitude below the wave breaking limit. The presence of a loading plasma changes the conventional free electron laser interaction mechanism. The space charge Langmuir mode (L) is parametrically driven by the nonlinear force of the wiggler (W) and the microwave (S) fields through the Raman (LWS) interaction. In turn, the coupling of the space charge mode with the wiggler field drives the microwave field. Also, the coupling of the electron beam (B) with the wiggler is another driving force to generate the microwave field through the free electron laser (BWS) interaction. This BWS interaction is a linear driving term in the fluid description of the beam, but is a nonlinear term in the single-particle description. Hence, the four enti-

ties (L,B,W,S) interact among themselves through two fundamental parametric processes. The simultaneous LWS and BWS coupling can be assured if the phase velocity of the beam-plasma mode matches the free electron laser resonant beam velocity. Although an axial magnetic guide field is not imposed, the machine parameters are within reach of experimental conditions.

II. BEAM-PLASMA MODE

With a fluid description, the density perturbations δN, δn of the background and the beam plasmas are given, respectively, by [9]

$$\left[\frac{\partial^2}{\partial t^2}+\frac{\omega_p^2}{\gamma}\right]\delta N=\frac{Nc^2}{4\gamma^2}\frac{\partial^2}{\partial z^2}\left(\frac{q\vec{A}}{mc^2}\cdot\frac{q\vec{A}}{mc^2}\right)-\frac{\omega_p^2}{\gamma}\delta n, \quad (1)$$

$$\left[\left(\frac{\partial}{\partial t}+v_z\frac{\partial}{\partial z}\right)^2+\frac{\omega_b^2}{\gamma_b}\right]\delta n=\frac{nc^2}{2\gamma_b^2}\frac{\partial^2}{\partial z^2}\left(\frac{q\vec{A}}{mc^2}\cdot\frac{q\vec{A}}{mc^2}\right)-\frac{\omega_b^2}{\gamma_b}\delta N, \quad (2)$$

where ω_p,ω_b are the plasma frequencies, γ,γ_b are the Lorentz factors of the background and the beam plasmas, respectively, and $q=-e$. The scalar potential of the space charge field is

$$\frac{\partial^2}{\partial z^2}\Phi=-4\pi q(\delta N+\delta n). \quad (3)$$

For a stationary background plasma, we have $\gamma=1$. However, in the presence of the wave field, γ can be slightly above unity. We note that the ponderomotive force term in Eq. (1) is only half of what it used to be in the Raman interaction formulation [9]. This is due to the fact that one of the waves we are considering is a static wiggler which does not drive a fluid velocity in a stationary background plasma.

We consider harmonic dependence such that $(\delta N,\delta n,\Phi)=(\delta N_0,\delta n_0,\Phi_0)\sin(\psi_L+\phi_j)$, where $\psi_L=(k_Lz-\omega_Lt)$ is the harmonic phase, and $\phi_j=(\phi_L,\phi_b,\phi_p)$ are the relative phases for the background plasma, the beam plasma, and the scalar potential, respectively. The linear dispersion relation of the beam-plasma mode, by neglecting $\vec{A}\cdot\vec{A}$ terms, is

$$\frac{\delta n_0}{\delta N_0}=\frac{\omega_L^2-\omega_p^2/\gamma}{\omega_p^2/\gamma}=\frac{\omega_b^2/\gamma_b}{(\omega_L-k_Lv_z)^2-\omega_b^2/\gamma_b}, \quad (4)$$

which can be written in the more familiar form

$$\frac{\omega_p^2/\gamma}{\omega_L^2}+\frac{\omega_b^2/\gamma_b}{(\omega_L-k_Lv_z)^2}=1. \quad (5)$$

The qualitative behavior of the dispersion relation is well known. It has two branches separated by the beam line $(\omega_L-k_Lv_z)=0$. The branch with $(\omega_L-k_Lv_z)>0$ consists of positive energy modes whereas the contrary has negative energy modes. Each branch goes asymptotically to the beam line in one end and to the Lamgmuir line $\omega_L=\omega_p/\gamma^{1/2}$ in the other. The beam-plasma mode is carried by two density perturbations $\delta n_0,\delta N_0$ as indicated by Eq. (4). Near the Langmuir frequency, δN_0 is much larger than δn_0, whereas at high frequencies, the inverse is true. The $(\omega_L-k_Lv_z)<0$ branch has two modes, which are called slow modes, with phase velocity less than the beam velocity v_z, whereas the $(\omega_L-k_Lv_z)>0$ branch has fast modes. The dispersion relation can be solved for the beam-plasma modes by iterations according to

$$\omega_L=k_Lv_z\pm\frac{\omega_b}{\gamma_b^{1/2}}\frac{1}{(1-\omega_p^2/\gamma\omega_L^2)^{1/2}}=k_Lv_z\pm\frac{\omega_b}{\gamma_b^{1/2}}\frac{1}{F(\omega_L)}, \quad (6)$$

where the upper sign is for the positive energy mode and the lower sign is for the negative energy mode. With a plasma-loaded wiggler, the device can operate in a frequency range far above the microwave range by choosing an adequate background plasma density, which is the major advantage of this device.

III. RAMAN AND FREE ELECTRON LASER INTERACTIONS

With the beam-plasma mode, it is able to drive an electromagnetic mode which is described by the following wave equation:

$$\left[\frac{\partial^2}{\partial t^2}-c^2\frac{\partial^2}{\partial z^2}+\omega_c^2\right]\vec{A}_s=-\left(\frac{\omega_b^2}{\gamma_b}+\frac{\omega_b^2}{\gamma_b}\frac{\delta n}{n}\right)\vec{A}_w-\left(\frac{\omega_b^2}{\gamma_b}\frac{\delta n}{n}+\frac{\omega_p^2}{\gamma}\frac{\delta N}{N}\right)\vec{A}_s, \quad (7)$$

where $\omega_c^2=(\omega_p^2/\gamma+\omega_b^2/\gamma_b)$ is the cutoff frequency squared and $\vec{A}_s=A_{s0}\sin(\psi_s+\phi_s)\hat{y}$, where $\psi_s=(k_sz-\omega_st)$ is the harmonic phase and ϕ_s is the relative phase. The linear dispersion relation is

$$\omega_s^2=\omega_c^2+c^2k_s^2. \quad (8)$$

Taking the wiggler field $\vec{A}_w=A_{w0}\sin\psi_w\hat{y}$, where $\psi_w=k_wz$, considering slowly varying amplitudes and the $\psi_L=\psi_s+\psi_w$ matching condition, Eq. (7) leads to

$$2\omega_s\left[\left(\frac{\partial}{\partial t}+v_g\frac{\partial}{\partial z}\right)A_{s0}\right]\cos(\psi_s+\phi_s)-2\omega_s\left[\left(\frac{\partial}{\partial t}+v_g\frac{\partial}{\partial z}\right)\phi_s\right]A_{s0}\sin(\psi_s+\phi_s)=\left[\frac{\omega_b^2}{\gamma_b}A_{w0}\sin(\psi_L+\phi_s)+\frac{\omega_b^2}{2\gamma_b}A_{w0}\frac{\delta n_0}{n}\cos\Delta\phi_b\right]\cos(\psi_s+\phi_s)-\left[\frac{\omega_b^2}{\gamma_b}A_{w0}\cos(\psi_L+\phi_s)+\frac{\omega_b^2}{2\gamma_b}A_{w0}\frac{\delta n_0}{n}\sin\Delta\phi_b-\delta_sA_{s0}\right]\sin(\psi_s+\phi_s), \quad (9)$$

where $v_g=c^2k_s/\omega_s$ is the group velocity, $\delta_s=(\omega_c^2+c^2k_s^2-\omega_s^2)$ is the frequency mismatch, and $\Delta\phi_b=(\phi_b-\phi_s)$. We note that

the second term on the right-hand side of Eq. (7) is nonresonant, and therefore this term is dropped. On the right-hand side of Eq. (9), the first terms in each square bracket, which are linear terms in A_{w0}, correspond to the linear transverse current as a result of the beam interaction with the wiggler. The phase bunching of these terms is the driving mechanism in standard free electron lasers. There are another two terms in $A_{w0}\delta n_0/n$ that arise from parametric interaction of the wiggler and the space charge field that corresponds to the Raman interaction.

The background plasma perturbation δN_0 of Eq. (1) becomes

$$2\omega_L\frac{\partial\delta N_0}{\partial t}\cos(\psi_L+\phi_L)-2\omega_L\frac{\partial\phi_L}{\partial t}\delta N_0\sin(\psi_L+\phi_L)=\left[-\frac{N}{4\gamma^2}c^2k_L^2\frac{qA_{w0}}{mc^2}\frac{qA_{s0}}{mc^2}\cos\Delta\phi_L+\frac{\omega_p^2}{\gamma}\delta n_0\sin\Delta\phi_{bL}\right]\cos(\psi_L+\phi_L)$$
$$-\left[\frac{N}{4\gamma^2}c^2k_L^2\frac{qA_{w0}}{mc^2}\frac{qA_{s0}}{mc^2}\sin\Delta\phi_L-\frac{\omega_p^2}{\gamma}\delta n_0\cos\Delta\phi_{bL}-\delta_L\delta N_0\right]$$
$$\times\sin(\psi_L+\phi_L), \tag{10}$$

where $\delta_L=[(\omega_p^2/\gamma)(\delta n_0/\delta N_0)+(\omega_p^2/\gamma)-\omega_L^2]$ is the frequency mismatch of the beam-plasma mode for the background space charge, $\Delta\phi_L=(\phi_L-\phi_s)$, and $\Delta\phi_{bL}=(\phi_b-\phi_L)$. Likewise, the beam perturbation δn_0 evolves as

$$2(\omega_L-k_Lv_z)\left[\left(\frac{\partial}{\partial t}+v_z\frac{\partial}{\partial z}\right)\delta n_0\right]\cos(\psi_L+\phi_b)-2(\omega_L-k_Lv_z)\left[\left(\frac{\partial}{\partial t}+v_z\frac{\partial}{\partial z}\right)\phi_b\right]\delta n_0\sin(\psi_L+\phi_b)$$
$$=\left[-\frac{n}{2\gamma_b^2}c^2k_L^2\frac{qA_{w0}}{mc^2}\frac{qA_{s0}}{mc^2}\cos\Delta\phi_b+\frac{\omega_b^2}{\gamma_b}\delta N_0\sin\Delta\phi_{Lb}\right]\cos(\psi_L+\phi_b)-\left[\frac{n}{2\gamma_b^2}c^2k_L^2\frac{qA_{w0}}{mc^2}\frac{qA_{s0}}{mc^2}\sin\Delta\phi_b\right.$$
$$\left.-\frac{\omega_b^2}{\gamma_b}\delta N_0\cos\Delta\phi_{Lb}-\delta_b\delta n_0\right]\sin(\psi_L+\phi_b), \tag{11}$$

where $\delta_b=[(\omega_b^2/\gamma_b)(\delta N_0/\delta n_0)+(\omega_b^2/\gamma_b)-(\omega_L-k_Lv_z)^2]$ is the frequency mismatch for the beam space charge, $\Delta\phi_b=(\phi_b-\phi_s)$, and $\Delta\phi_{Lb}=(\phi_L-\phi_b)$. In order to describe the energy deplection of the beam, we introduce the beam energy equation to complete the fluid description,

$$\left(\frac{\partial}{\partial t}+v_z\frac{\partial}{\partial z}\right)\gamma_b^2=-\omega_s\frac{qA_{w0}}{mc^2}\frac{qA_{s0}}{mc^2}[\sin(\psi_L+\phi_s)-\sin(\psi_L+\phi_s-2\psi_w)]$$
$$-2\frac{\gamma_b\beta_z}{ck_L}\left(\omega_p^2\frac{\delta N_0}{N}\cos(\psi_L+\phi_L)+\omega_b^2\frac{\delta n_0}{n}\cos(\psi_L+\phi_b)\right). \tag{12}$$

The first term on the right-hand side of Eq. (12) accounts for the electromagnetic transverse electric field, whereas the second term amounts to the electrostatic longitudinal field. Here, in Eqs. (10) and (11), the parametric Raman interaction of the wiggler and the microwave field, in turn, drives the space charge field with the beam energy consistently calculated by Eq. (12). Together with Eq. (9), they form a closed system to study the emission of high-frequency fields.

IV. SINGLE-PARTICLE DESCRIPTION

We remark that the matching condition for the Raman interaction $\psi_L=\psi_s+\psi_w$ leads to the following phase velocity of the space charge $\omega_L/k_L=\omega_s/(k_s+k_w)$. For the free electron laser interaction, we require $(\omega_s-k_sv_R)=k_wv_R$, which states that the Doppler shifted laser frequency in the beam frame be equal to the wiggler frequency at the resonant beam velocity v_R. The Raman interaction and the free electron laser interaction, therefore, take place simultaneously when

$$\frac{\omega_L}{k_L}=\frac{\omega_s}{k_s+k_w}=v_R,$$

which calls for the space charge phase velocity to be set to the resonant velocity.

The fluid description of the preceding section offers a complete set of equations to deal with this. Here we set up an alternative single-particle description of the beam electrons to compare the results. Representing the electron beam in the ponderomotive well by $(2N+1)$ ensemble electrons with energy γ_j and phase $\psi_j=(\psi_s+\psi_w)_j$, where $-N\leqslant j\leqslant+N$, we have

$$\left(\frac{\partial}{\partial t}+v_z\frac{\partial}{\partial z}\right)\gamma_j^2=-\omega_s\frac{qA_{w0}}{mc^2}\frac{qA_{s0}}{mc^2}[\sin(\psi_j+\phi_s)-\sin(\psi_j+\phi_s-2\psi_w)]$$
$$-2\frac{\gamma_j\beta_j}{ck_L}\left(\omega_p^2\frac{\delta N_0}{N}\cos(\psi_j+\phi_L)+\omega_b^2\frac{\delta n_0}{n}\cos(\psi_j+\phi_b)\right), \tag{13}$$

$$\left(\frac{\partial}{\partial t}+v_z\frac{\partial}{\partial z}\right)\psi_j=ck_L(\beta_{zj}-\beta_L), \tag{14}$$

where $\beta_L=\omega_L/ck_L$. The density perturbation can be expressed in terms of the Fourier components of $(\psi_L-\psi_j)$ in the phase space as

$$\frac{\delta n}{n}=2\sum_{m=1}^{\infty}\langle\cos\, m(\psi_L-\psi_j)\rangle_j. \tag{15}$$

Here, the angular brackets represent the average over an ensemble of beam electron j in the ponderomotive well, and the sum is over the Fourier harmonics m. In our calculations, we sum over twenty harmonics. The beam energy in this description is given by $\gamma_b=\langle\gamma_j\rangle$. From Eq. (15), the amplitudes of the density perturbation and the relative phase are given by

$$\left(\frac{\delta n_0}{n}\right)^2=4\left[\left(\sum_{m=1}^{\infty}\langle\sin\,\Psi_{mj}\rangle_j\right)^2+\left(\sum_{m=1}^{\infty}\langle\cos\,\Psi_{mj}\rangle_j\right)^2\right], \tag{16}$$

$$\tan\,\Delta\phi_{bL}=-\frac{\Sigma_{m=1}^{\infty}\langle\cos\,\Psi_{mj}\rangle_j}{\Sigma_{m=1}^{\infty}\langle\sin\,\Psi_{mj}\rangle_j}, \tag{17}$$

where $\Psi_{mj}=[m(\psi_L-\psi_j)-(\psi_L+\phi_L)]$. The linear transverse current, J_y, on the right-hand side of Eq. (9) is now given by

$$-(4\pi c)J_y=\omega_b^2A_{w0}\left[\left\langle\frac{1}{\gamma}\sin(\psi_j+\phi_s)\right\rangle_j\cos(\psi_s+\phi_s)-\left\langle\frac{1}{\gamma}\cos(\psi_j+\phi_s)\right\rangle_j\sin(\psi_s+\phi_s)\right]. \tag{18}$$

We recall that, in the fluid description, the A_{w0} term in Eq. (9) is a linear term, but, in the single-particle description, this term given by Eq. (18) is a nonlinear phase bunching term in free electron lasers. We also remark that, although Eqs. (12) and (13) are identical in form, they are different in essence. The beam density perturbation in the fluid description is derived from density and momentum continuity equations, whereas it is calculated from phase bunching in the ponderomotive well in the single-particle description. Consequently, $\delta n_0/n$ and ϕ_b are evaluated entirely differently in the two versions of the beam energy equation.

We consider a beam much longer than the wiggler length so that leading and trailing edge effects can be neglected [10]. The beam equations, Eqs. (11) and (12) or Eqs. (13) and (14), can be transformed to the beam characteristic to follow the fixed group of ensemble electrons in the ponderomotive well [11]. By the same token, the electromagnetic field, Eq. (9), can be represented along the wave characteristic to follow the same wave packet. By taking $v_g=v_z$, the two characteristics are the same, and the slippage effect can be neglected [10]. The description along the characteristic is equivalent to the Lagrangian representation of the fluid element. The space charge field equation, Eq. (10), describes a density perturbation that propagates with the phase velocity equal to the resonant beam velocity. The trajectory of the space charge phase is given by $z=v_Rt$. On the beam frame, the electron, therefore, follows the same space charge potential. Since the growth of the amplitude is uniform in space, the time derivative of Eq. (10) can be written as a convective derivative in the beam frame. Consequently, Eqs. (9)–(14) reduce to the first-order ordinary differential equations with respect to the fixed beam element as it traverses the wiggler.

V. SYSTEM PARAMETERS

The operation of a plasma-loaded-wiggler free electron device requires careful choice of the system parameters that are consistent with the simultaneous interaction of the Raman scattering and the free electron laser resonance. We take the primary input parameters as the background plasma density N, the beam density n, the beam energy γ_b, and the wiggler period λ_w. The beam velocity β_z can be calculated as a function of the beam energy γ_b. The beam-plasma mode ω_L and the laser mode ω_s satisfy Eqs. (5) and (8), respectively. Solving k_L and k_s from their respective dispersion relations, and making use of the matching condition $k_L=k_s+k_w$, we have the mode frequency $\omega=\omega_L=\omega_s$ given by

$$\omega=\gamma_b^2\omega_w\pm[(\gamma_b^2\omega_w)^2-\gamma_b^2(\omega_w^2+\beta_z^2\omega_c^2)]^{1/2}, \tag{19}$$

$$\omega_w=k_wv_z\pm\frac{\omega_b}{\gamma_b^{1/2}}\frac{1}{F(\omega)}, \tag{20}$$

where the function $F(\omega)$ is defined in Eq. (6). The upper sign of Eq. (20) is for the $(\omega-kv_z)>0$ branch, and the lower sign is otherwise. For a given branch, Eq. (19) gives a high-frequency mode with the upper sign, and a lower-frequency mode otherwise. In order to have real frequencies, the radical in Eq. (19) has to be positive. The primary system parameters are, therefore, subjected to the constraint

$$\gamma_b\omega_w>\omega_c. \tag{21}$$

Since the mode frequency ω_s is determined by the background and beam-plasma densities, the frequency mismatches are zero initially. However, there are energy factors such as $\gamma=(1+a_s^2/2)$ and γ_b which vary down the wiggler. These effects are calculated consistently in our equations through the frequency mismatches.

VI. TWO-STREAM INSTABILITY

We consider specifically $N=1\times10^{14}/\mathrm{cm}^3$, $n=7\times10^{12}/\mathrm{cm}^3$, $\alpha=n/N=7\times10^{-2}$, $\gamma_b=5$, and $\lambda_w=1$ cm. The background plasma frequency is $\omega_p=5.6\times10^{11}$ rad/s, and the beam mode frequency is $\omega_L=(12.4/3.6)\times10^{12}$ rad/s for the positive/negative branch, respectively. As the initial con-

ditions, we take $a_p=\delta N_0/N=0$, $\phi_L=0$ for the background plasma. As for the beam, we have $a_b=\delta n_0/n=0$ $\phi_b=0$, for the fluid description, and ψ_j is random between $(-\pi, +\pi)$, $\gamma_j=\gamma_b$, for the single-particle description. For the electromagnetic field, we take $a_s=qA_{s0}/mc^2=0$, $\phi_s=0$. The wiggler length is chosen as $L=100\lambda_w$. For the wiggler strength, $a_w=qA_{w0}/mc^2=0.1$, which corresponds to a wiggler magnetic field of $B_{w0}=1$ kG, is sufficient to drive the system in the fluid model. However, in the single-particle model, $a_w=1.0$ with $B_{w0}=10$ kG is required. We integrate Eqs. (9) and (10) together with either Eqs. (11) and (12) or Eqs. (13) and (14) along the wiggler to follow the evolutions of γ_b, a_b, a_p, a_s. In each wiggler period, we use 30 000 grid points for the fluid model, and 600 for the single-particle model.

Before presenting the four-entity interactions, we first consider the classical two-stream interaction by setting $a_w=0$ and $a_s=0$ to verify the consistency of our equations. We first neglect the beam energy equation, Eq. (12), and only integrate Eqs. (10) and (11) as in the textbook case. We choose the low-frequency positive energy mode such that the wave vector corresponding to this frequency falls in the interval of the dispersion curves where complex roots are expected. To avoid numerical overflow, an infinitesimal noise level is assigned to the space charge field initially. With $\alpha=7\times10^{-2}$, numerical results indicate that the space charge is unable to grow beyond the noise level due to the low beam-plasma ratio. To show the two-stream instability, we exceptionally lower the background plasma density to raise the beam-plasma ratio. Taking $N=1\times10^{13}/cm^3$ with $\alpha=0.7$, the space charge field now grows exponentially, just according to the linear theory, until numerical overflow is reached. By introducing Eq. (12) to account for the energy depletion of the driving beam, the space charge field soon saturates with the energy depletion of the beam. For high-frequency modes in both the positive and the negative branches, the space charge field fails to grow beyond the initial noise level even with $\alpha=0.7$ as expected by the linear theory since all the roots are real.

VII. *LBWS* INTERACTION

Having examined the two-stream instability, we now return to the original machine parameters with $\alpha=7\times10^{-2}$. Applying the wiggler field with $a_w=0.1$, and considering the electromagnetic field equation and the beam energy equation, Fig. 1 shows the results of the fluid description, Eqs. (9)–(12), with the high-frequency negative energy mode at the frequency $f=5.8\times10^{11}$ Hz as a function of the normalized wiggler distance z/λ_w. Unlike the preceding section, the space charge field a_p in Fig. 1(c), driven by the parametric force of the $a_{w0}a_{s0}$ term, is readily excited at a low beam-plasma ratio for the high-frequency beam mode. The beam energy γ_b in Fig. 1(a) declines as the electromagnetic field intensity a_s^2 in Fig. 1(b) increases. To understand the results of Fig. 1 and Figs. 2–4 that follow, we recall that we are dealing with a four-entity interaction, instead of three, where the wiggler has a constant amplitude. In our four-entity interaction, there are two channels of three-entity parametric interaction. Energies can interchange between these channels. Initially, the beam transfers energy to the electromagnetic field parametrically through the wiggler (*BWS*) stated by Eq. (9). This is followed by the excitation of the space charge mode by the parametric action of the electromagnetic field and the wiggler (*LWS*) as in Eqs. (10) and (11). As the space charge mode gets large enough, it can overcome the parametric term in Eq. (12) to determine the beam energy. Furthermore, the space charge field interacts parametrically with the wiggler to drive a feedback to the electromagnetic field as shown in the space charge terms on the right side of Eq. (9). The solution of this four-entity system is determined by the energy equipartition among all these channels. In this spirit, we see that the beam drives slowly the electromag-

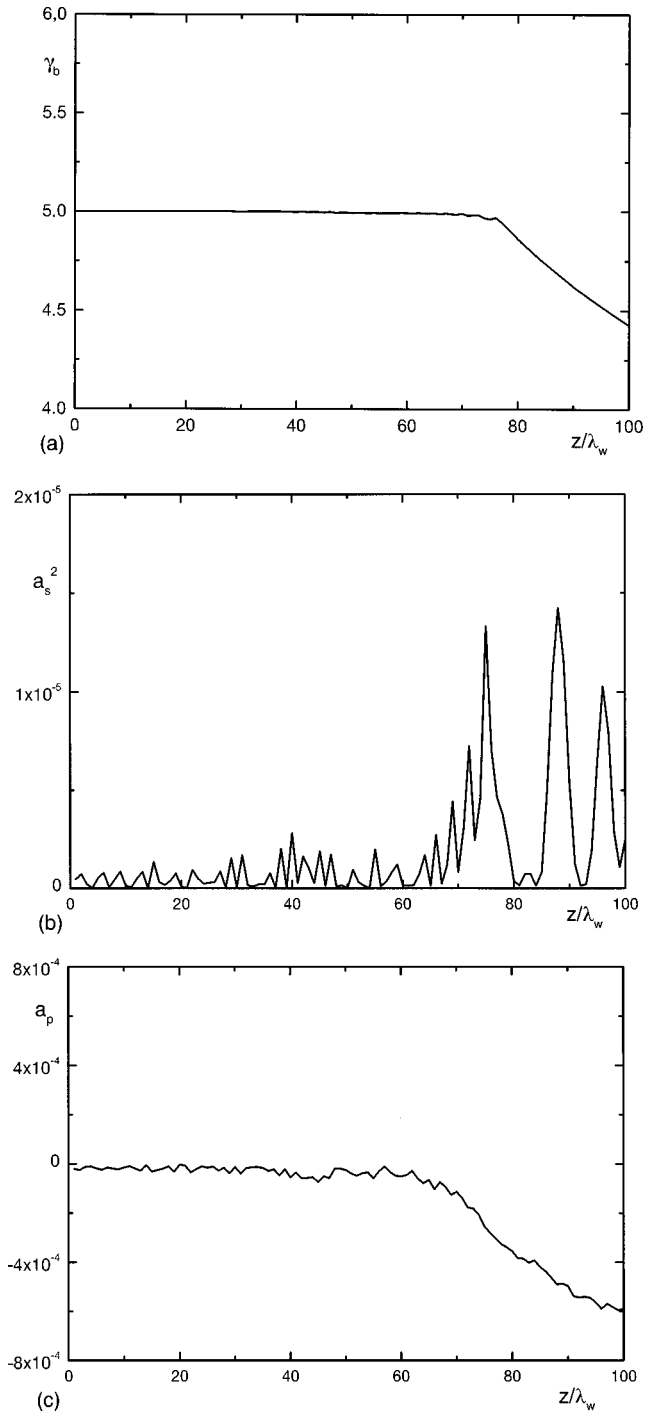

FIG. 1. (a) γ_b, (b) a_s^2, (c) a_p of the negative energy high-frequency mode in the fluid description as a function of z/λ_w.

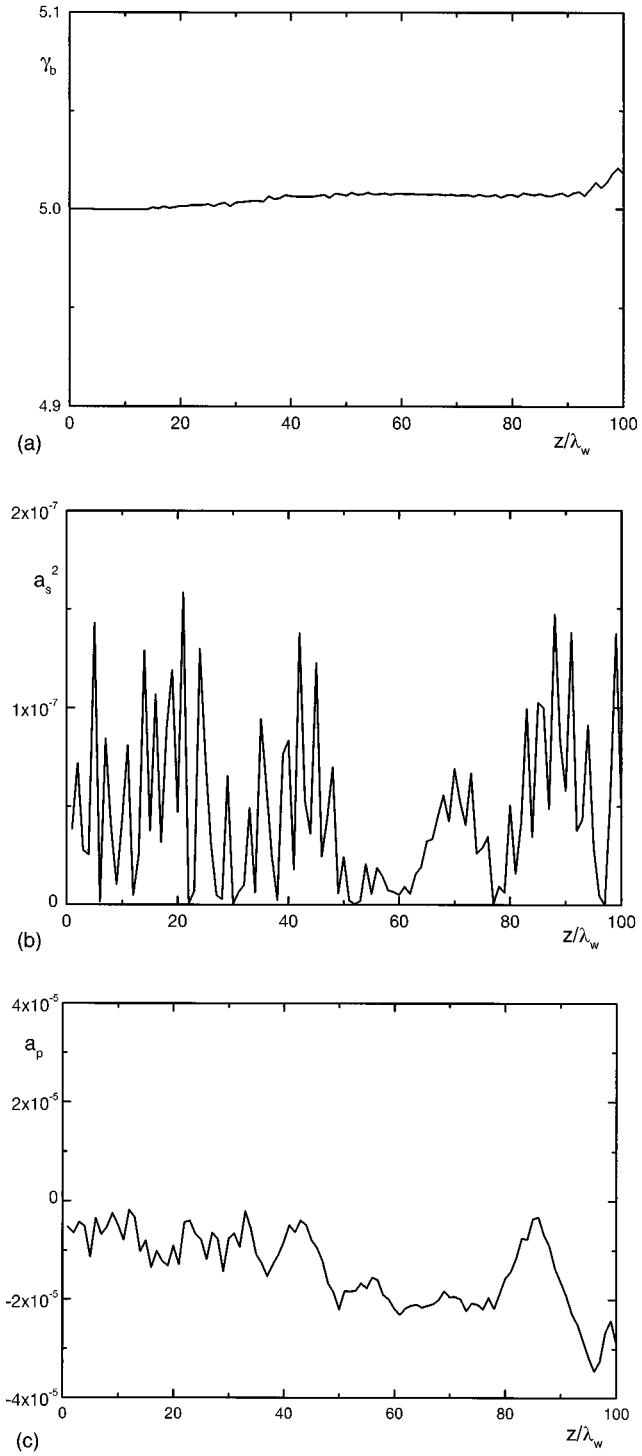

FIG. 2. (a) γ_b, (b) a_s^2, (c) a_p of the positive energy high-frequency mode in the fluid description as a function of z/λ_w.

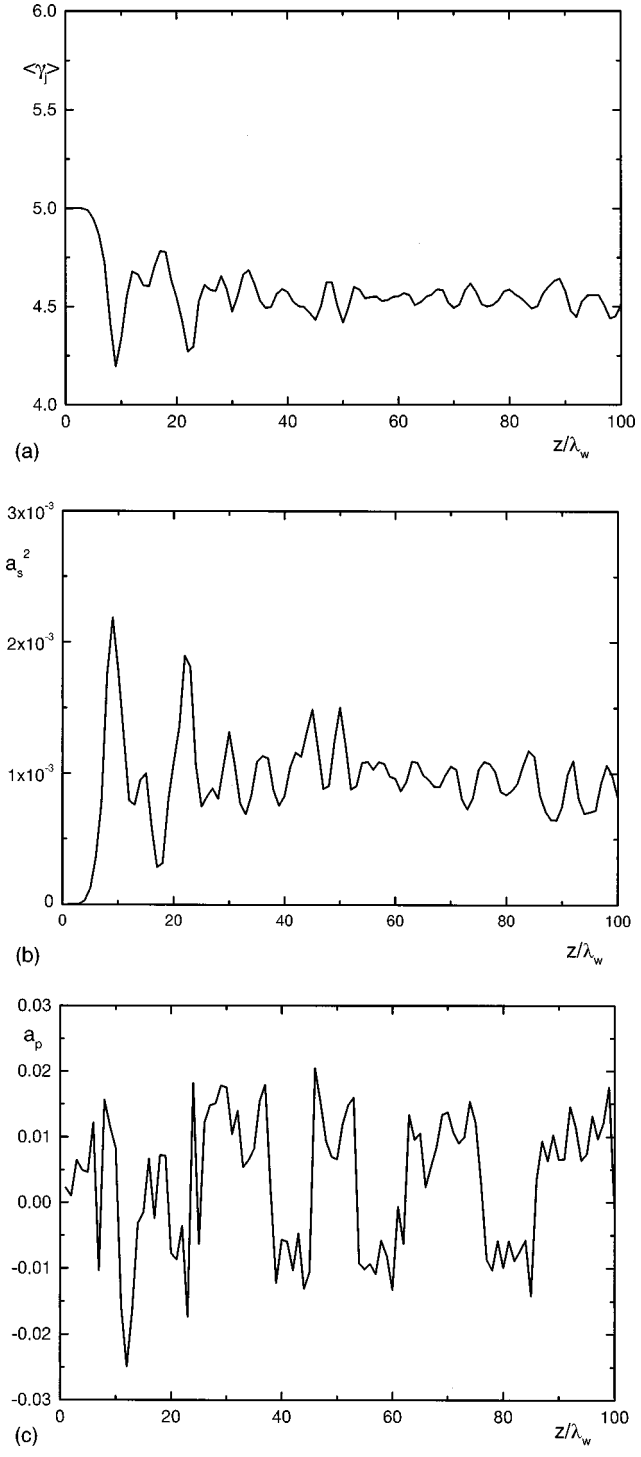

FIG. 3. (a) γ_b, (b) a_s^2, (c) a_p of the negative energy high-frequency mode in the single-particle description as a function of z/λ_w.

netic mode up to the seventieth wiggler dominated by the *BWS* process. From there on, the space charge field is enhanced through the *LWS* process with reduction on the electromagnetic mode. The combined effect of the space charge mode and the parametric term acts in such a way to drive the beam energy down to $\gamma=4.1$. In Fig. 2, the results of the high-frequency positive energy beam mode at the frequency $f=1.9\times10^{12}$ Hz show beam energy above the initial level, a weak electromagnetic field, and a larger space charge field. In this case, the *BWS* interaction is effective in the first twenty wigglers followed by the *LWS* interaction. The space charge term in Eq. (12) acts electrostatically to accelerate the beam slightly.

VIII. SINGLE-PARTICLE RESULTS

We now consider the single-particle description by integrating Eqs. (9), (10), (13), and (14) with the corresponding evaluations of Eqs. (15)–(18). We first make a remark about

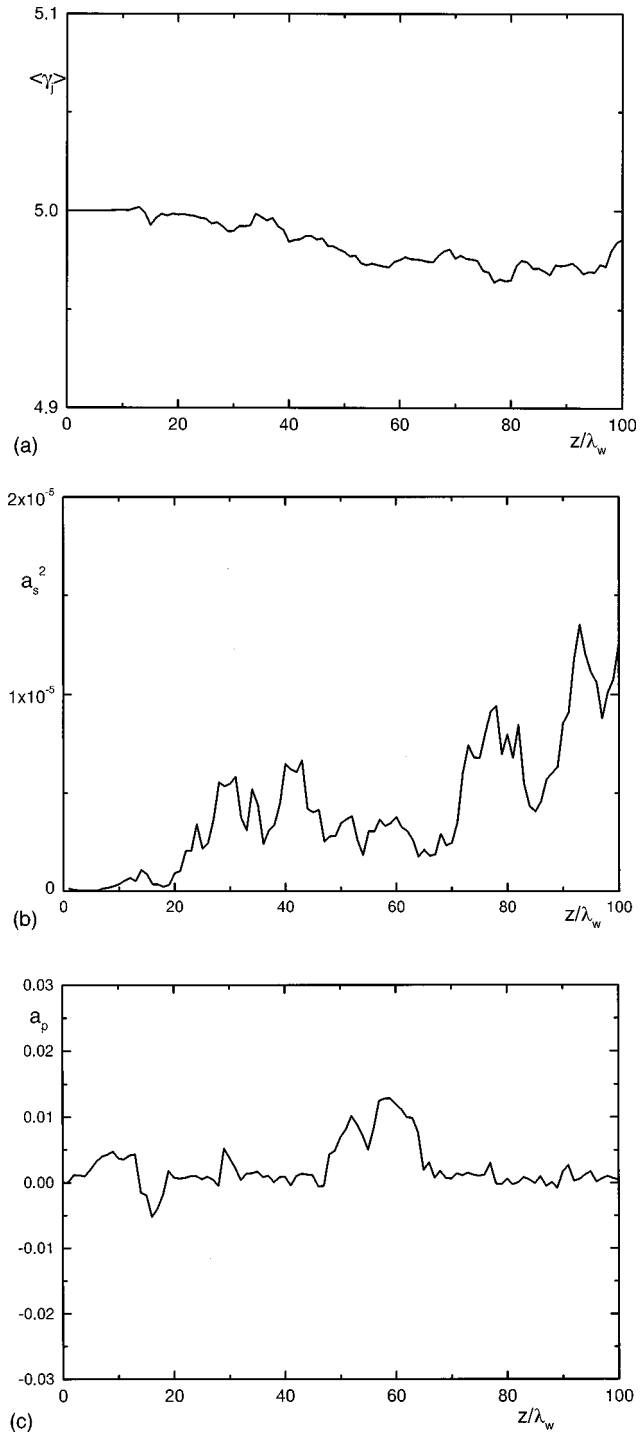

FIG. 4. (a) γ_b, (b) a_s^2, (c) a_p of the positive energy high-frequency mode in the single-particle description as a function of z/λ_w.

the choice of a random initial phase distribution for ψ_j between $(-\pi, +\pi)$ to simulate the beam in the single-particle description. Such a choice is to eliminate the effect of beam lethargy to emit microwaves. In standard free electron lasers, we often attribute a uniform initial phase to ψ_j to evaluate their output. When the beam energy is almost equal to the resonant energy, this distribution is known to give lethargy since the electrons take a long time to leave the uniform distribution. When the beam energy is different from the resonant energy by a small fraction, the electrons are easily driven in the ponderomotive well by this energy difference. Beam lethargy is unimportant and the details of the initial distribution are irrelevant. In our system here, the beam energy and the resonant energy are very close, such that the initial phase distribution of the electrons would make a significant difference on the device performance. From the physical point of view, it is more reasonable to think of the electrons in the ponderomotive well with a random phase initially than with a uniform phase. We therefore prefer a random distribution which has a minimum beam lethargy compared to the uniform distribution, and we expect that the nature is better represented by the random distribution than otherwise.

For the single-particle description, if we use $a_w = 0.1$ as in the fluid model, we would not get any yield comparable to Figs. 1(b) and 2(b). This is due to the weak bunching on the transverse current of Eq. (18). With $a_w = 1.0$, and for the high-frequency negative energy mode, the system performance is shown in Fig. 3. The beam energy in Fig. 3(a) shows oscillations about a certain beam energy level. The electromagnetic intensity in Fig. 3(b) has a good output, while the space charge mode in Fig. 3(c) oscillates with large amplitudes. Numerical results indicate that the electromagnetic intensity stays at the level reached in Fig. 3(b) even if more wigglers are added to the system. With $\omega_s = 3.6 \times 10^{12}$ rad/s and $a_s^2 = 3 \times 10^{-3}$, the energy flux of the electromagnetic mode is approximately 10 MW/cm^2. Since the maxima of Fig. 3(b) coincide with the minima of Fig. 3(a), the major process that takes place in the system is the *BWS*. The electromagnetic mode grows at the expense of the beam energy and the space charge feedback in Eq. (9). The details of these results vary quantitatively with the choice of the seed in the random number generator, although the orders of magnitude are seldom affected. For the high-frequency positive energy mode, Fig. 4 shows a situation different from Fig. 2, in which the beam energy drops slightly below its initial value. The electromagnetic mode of Fig. 4(b) is much weaker than its counterpart in Fig. 3(b).

To summarize, the negative energy mode is adequate to generate powerful terahertz electromagnetic radiation, although the wiggler strength required in this operation differs from one description to another, whereas the positive energy mode is not suitable for this purpose in both descriptions. To interpret these qualitative behaviors, we recall that the resonant energy of the positive mode is slightly higher than the beam energy. During the four-entity interaction, the space charge mode and the electromagnetic mode are the pumps to drive the beam according to Eq. (12) or Eq. (13). Depending on the strength and phase of each pump, the beam can either gain or lose a little bit of energy. Since both the space charge and electromagnetic modes are zero initially, the underlying energy source is the wiggler which has its strength maintained constant externally. For the negative mode, the resonant energy is slightly lower than the beam energy. The beam, therefore, is the pump to drive the electromagnetic mode and the space charge mode, with the help of the wiggler.

IX. DISCUSSION AND CONCLUSIONS

We have analyzed the performance of a plasma-loaded-wiggler free electron device based on the fluid and single-

particle descriptions. Only the high-frequency positive and negative energy modes are studied. The low-frequency modes are not desirable, not just for the fact that they operate at lower frequencies, but, with unsuitable choice of wiggler period, the low-frequency positive energy mode could fall in the unstable domain of the beam-plasma dispersion relation, which makes the device highly unstable. In the fluid description, the system is able to operate with a small wiggler field in contrast to the single-particle description, where the wiggler field has to be increased tenfold. This substantial difference between the two models originates from the a_{w0} terms on the right-hand side of Eq. (9), which represents the transverse current. In the fluid description, this term is a linear growth term which allows the electromagnetic mode to get an initial start. In the single-particle description, this term is a nonlinear term that relies on the phase bunching of the beam electrons. In order to reach comparable effects in the fluid model, the magnetic field has to be substantially increased. We believe that the fluid description offers overestimated performances, and the single-particle description provides more reliable results. Unlike the three-entity interaction, our $LBWS$ interaction contains several energy channels, and the steady state of this system is governed by the energy equipartition of these channels. Numerical results indicate that this is a promising device to generate terahertz fields.

ACKNOWLEDGMENTS

This work was partially supported by the Conselho Nacional de Desenvolvimentos Cientifico e Tecnologico (CNPq, The Brazilian National Council of Scientific and Technologic Developments).

[1] T. J. Orzechowski, B. R. Anderson, J. C. Clark, W. M. Fawley, A. C. Paul, D. Prosnitz, E. T. Scharlemann, S. M. Yarema, D. B. Hopkins, A. M. Sessler, and J. S. Wurtele, Phys. Rev. Lett. **57**, 2172 (1986).

[2] M. E. Conde and G. Bekefi, Phys. Rev. Lett. **67**, 3082 (1991).

[3] H. H. Szu, IEEE J. Quantum Electron. **19**, 379 (1983).

[4] J. L. Bobin, Opt. Commun. **55**, 413 (1985).

[5] P. Wen-Bing and C. Ya-Shen, Int. J. Electron. **65**, 551 (1988).

[6] V. K. Tripathi and C. S. Liu, IEEE Trans. Plasma Sci. **18**, 466 (1990).

[7] A. Serbeto and M. V. Alves, IEEE Trans. Plasma Sci. **21**, 243 (1993).

[8] V. Petrillo, A. Serbeto, C. Maroli, R. Parrella, and R. Bonifacio, Phys. Rev. E **51**, 6293 (1995).

[9] D. W. Forslung, J. M. Kindel, and E. L. Lindman, Phys. Fluids **18**, 1002 (1975).

[10] K. H. Tsui, Phys. Fluids B **5**, 3808 (1993).

[11] R. Courant and D. Hilbert, *Methods of Mathematical Physics* (Interscience, New York, 1962), Vol. II, Chap. II.